Indonesian Journal of Biotechnology

VOLUME 28(3), 2023, 180-190 | RESEARCH ARTICLE

Computational approaches to identify novel inhibitors for the drug-resistant *Mycobacterium tuberculosis* DprE1 enzyme

Chaitali Dhande[1,£], Devanshi Mistry[2,£], Anandakrishnan Karthic[3,£], Rajshri Singh[3,4], Sagar Barage[3,5,*]

[1]School of Biotechnology and Bioinformatics, D.Y. Patil University, CBD Belapur, Navi Mumbai – 400614, Maharashtra, India
[2]Institute of Chemical Technology (ICT), Mumbai - 400019, Maharashtra, India
[3]Amity Institute of Biotechnology, Amity University, Mumbai - Pune Expressway, Bhatan, Post-Somathne, Panvel - 410206, Maharashtra, India
[4]Centre for Proteomics and Drug Discovery, Amity University, Mumbai - Pune Expressway, Bhatan, Post-Somathne, Panvel - 410206, Maharashtra, India
[5]Centre for Computational Biology and Translational Research, Amity University, Mumbai - Pune Expressway, Bhatan, Post-Somathne, Panvel - 410206, Maharashtra, India
*Corresponding author: sagarbarage@gmail.com
[£]All authors equally contributed

SUBMITTED 15 December 2022 **REVISED** 17 July 2023 **ACCEPTED** 2 August 2023

ABSTRACT *Mycobacterium tuberculosis* causes tuberculosis (TB), which is a common but life-debilitating disease. The continued development of resistance to frontline anti-TB drugs such as isoniazid and rifampicin threatens the efficacy of currently available treatment procedures. This highlights the need to explore diverse approaches essential for drug development against multi-drug-resistant strains of tuberculosis. Drug development relies on the findings associated with novel protein targets, which play a crucial role in the disease life cycle. DprE1, an enzyme that plays a critical role in the cell wall synthesis of *M. tuberculosis*, has been recognized as a promising target for drug development. In the present study, based on previous experimental findings, seven mutant models of DprE1 involved in DprE1 resistance are predicted using homology modeling. Further, potential inhibitors are selected based on their efficacy and IC_{50} values. Shortlisted inhibitors are docked with the wild-type and mutant structures of DprE1. The deduced inhibitor molecule (ZINC5) is found to possess high potential as a lead inhibitor for all the models of DprE1. It can be used to circumvent drug resistance in the current treatment regime.

KEYWORDS DprE1; Drug resistant TB; *Mycobacterium*; Novel inhibitor; Tuberculosis (TB)

1. Introduction

The bacillus *Mycobacterium tuberculosis* affects millions of people worldwide, mainly by causing tuberculosis (TB). Among the deaths that occurred due to infectious diseases, TB was one of the leading causes (Kim et al. 2020). With advancements in science and technology, the number of TB cases worldwide has been decreasing in the last two decades (Kyu et al. 2018). However, in 2018, the World Health Organization estimated 10 million new cases of TB and 1.45 million deaths (Liu et al. 2020), with a reported number of 1,300,000 TB deaths in HIV-negative patients and 300,000 TB deaths in HIV-positive patients (Hariguchi et al. 2020). In spite of advancements in the treatment of the disease, there is persistence in the number of TB cases worldwide. It is a result of the significant emergence of multi-drug-resistant (MDR) and extensively drug-resistant (XDR) strains of *M. tuberculosis* (Wilsey et al. 2013). Novel target identification and novel drug development are the two potential approaches that scientists are focusing on to achieve effective treatment for the disease. The novel drug development approach is used to identify suitable agents against a known target with the help of computer-aided drug discovery (CADD). This pathway includes methods like quantitative structure-activity relationship (QSAR), virtual screening, molecular docking, molecular dynamics simulation, etc. In the past several years, multiple druggable targets of *M. tuberculosis* have been identified and tested for clinical use (Maharaj et al. 2015).

Mycobacterium tuberculosis has multiple drug targets, among them decaprenylphosphoryl-β-D-ribose 2'-epimerase (DprE1), flavoenzyme that is essential for mycobacterial cell wall biogenesis (Bhat et al. 2017). As a part of the decaprenylphosphoryl-β-D-arabinofuranose (DPA) pathway, oxidoreductase DprE1

followed by reductase DprE2 catalyse the epimerization of decaprenylphosphoryl-β-D-ribofuranose (DPR) to DPA. Inhibition of DprE1 halts the synthesis of DPA, which subsequently reduces the formation of arabinan, an important cell wall component (Oh et al. 2021). Therefore, *M. tuberculosis* cell wall synthesis is prevented due to the depletion of DPA, a necessary precursor for the synthesis of arabinan (Maharaj et al. 2015; Wilsey et al. 2013). Hence, DprE1 is one of the most studied protein targets for drug development against *M. tuberculosis*. However, the polymorphism and mutation in DprE1 confound the current treatment with the problem of drug resistance (Neres et al. 2015; Foo et al. 2016). Thus, it is essential to develop a novel DprE1 inhibitor for its potential use against MDR- and XDR- *M. tuberculosis*.

In the present study, we employed in silico approaches to discover novel inhibitors for the *M. tuberculosis* target protein DprE1, incorporating recently identified mutant residues. Subsequently, virtual screening has been performed to identify potential compounds with good binding affinity against DprE1 target. The identified novel inhibitor molecule will be acting as potential inhibitor and overcome the drug resistance in *M. tuberculosis*.

2. Materials and Methods

2.1. Homology modelling of wild-type and mutant DprE1

The protein sequence of DprE1 (UniProt ID P9WJF0) was retrieved from the UniProt protein sequence database (https://www.uniprot.org, The UniProt Consortium (2021)). There are two reviewed entries composed of 461 AA residues. Further, both sequences are 100% identical. Therefore, we selected one entry, P9WJF0, for our study. The template search was performed using BLASTp against the PDB database (https://www.rcsb.org). There are a total of 27 structures of DprE1 available in the PDB with different resolutions. However, all crystal structures are not full length and have unmodelled regions. From the obtained results, the structure of 4P8C.pdb (Neres et al. 2015) was selected for further studies as it shows 100% identity with the query sequence. Anyway, this structure lacks coordinates for amino acid regions 1–7, 268–274, and 323–326. The initial regions 1–6 are not involved in the interaction with the ligand. However, the 268–274 and 323–326 regions near the catalytic groove of DprE1 might be involved in the interaction with the ligand molecule (Neres et al. 2015). Therefore, these regions were modelled by the loop modelling option of Discovery Studio version 3.5 (Barage and Sonawane 2014; Barage et al. 2017). Finally, 20 homology models of DprE1 were generated using the MODELLER 10.2 program based on the obtained template structure. Among them, a single model was selected on the basis of the discrete optimized protein energy (DOPE) score (Webb and Sali 2021). The structural validation and characterization of the predicted models were performed using the PROCHECK and ERRAT tools available on the SAVES v6.0 server (https://saves.mbi.ucla.edu). Further, the ProSA-web server was also used to measure the protein quality (Laskowski et al. 1993; Wiederstein and Sippl 2007). Subsequently, the selected model was used to generate the mutant models. Based on previous experimental studies (Makarov et al. 2009; Neres et al. 2015; Foo et al. 2016), mutant structures were prepared by replacing wild-type residues with mutant residues. We used Discovery Studio (https://www.3ds.com/products-services/biovia/products/molecular-modeling-simulation/biovia-discovery-studio) for incorporating mutant residues in the model, minimizing compounds, and generating 2D and 3D interactions of ligands. The predicted structure of the wild-type enzyme was named DprE1-WT, while the mutant structures were named MutC387A, MutG17C, MutL368P, MutC387S, MutC387T, MutC387G, MutC387N and Mut-All (MutG17C, MutL368P, MutC387A), indicating Mut-original residue-amino acid position-mutated residue (Makarov et al. 2009; Neres et al. 2015; Foo et al. 2016). All of the generated mutant and wild-type models were subjected to energy minimization using the CHARMM force field (http://mackerell.umaryland.edu/charmm_ff.shtml). Subsequently, all models were used for docking studies.

2.2. Preparation of ligand dataset

All known DprE1 inhibitors were retrieved from previous experimental reports. The inhibitors PBTZ169, BTZ043, Azaindole and BTO were shortlisted based on their lowest IC_{50} values (Table 1). These shortlisted inhibitors were used for similarity searches against the ZINC database by setting the Tanimoto index to 90 (Sterling and Irwin 2015). From the obtained ligands, only purchasable ligands were extracted in (.sdf) format. In total, 46 ligand data sets were prepared, which include 42 similar and 4 known inhibitors, as listed in Table 2. All retrieved ligand molecules were loaded in PyRx through Open Babel and minimized using the MMFF94 force field (Dallakyan and Olson 2015). The minimized compounds were converted to an autodock compatible format (.pdbqt). The protonation state and Gasteiger charges were assigned to all ligand atoms.

2.3. Target preparation and virtual screening

Molecular docking studies were carried out using AutoDock 4.2, implemented in PyRx (Dallakyan and Olson 2015). The docking protocol has been validated using a redocking experiment in which the crystallographic pose of Y22 was separated from DprE1 (4P8C.pdb) and redocked into the active site of DprE1. The predicted binding mode of Y22 was compared with the crystallographic pose of Y22 using RMSD calculations (Barage et al. 2017; Meshram et al. 2020). The present docking protocol successfully reproduced the crystallographic position, and the same has been used for the unknown ligand molecules. The model of DprE1-WT was loaded in PyRx, and the charges and protonation states were

TABLE 1 Highest populated clusters (HPC) and binding energies (BE) of the top ligands in nine models of DprE1.

Model	Wild-type		C387A		C387G		C387N		C387T		C387S		L368P		G17C		Mut-All	
Ligand	HPC	BE	HPC	BE	HPC	BE	HPC	BE	HPC	BE	HPC	BE	HPC	BE	HPC	BE	HPC	BE
BTZ043	9	-9.18	30	-10.64	44	-9.88	**42**	**-9.88**	**64**	**-9.85**	20	-9.96	32	-10.54	19	-10.61	24	-10.54
PBTZ169	**15**	**-9.08**	34	-10.48	37	-10.74	29	-10.28	**56**	**-10.36**	**27**	**-10.44**	**51**	**-10.71**	28	-10.65	21	-9.83
ZINC5	**20**	**-10.38**	**55**	**-11.86**	**54**	**-11.12**	38	-8.91	**43**	**-10.12**	**28**	**-10.69**	**58**	**-11.54**	**34**	**-10.43**	**35**	**-11.63**
ZINC7	9	-9	28	-9.21	28	-9.07	32	-8.77	37	-8.9	25	-9.15	32	-8.75	29	-8.67	**35**	**-9.09**
ZINC8	**16**	**-10.25**	33	-9.1	38	-9.23	33	-8.81	24	-9.23	26	-8.99	41	-9.1	30	-9.18	29	-9.06
ZINC10	8	-9.01	27	-9.49	32	-9.71	**48**	**-8.89**	23	-9.11	27	-9.15	29	-9.69	**35**	**-9.36**	20	-9.46
ZINC17	12	-8.1	32	-8.85	**47**	**-8.75**	24	-9.84	41	-9.04	25	-8.86	29	-8.87	26	-8.51	**37**	**-8.69**
ZINC28	8	-9.73	**44**	**-10.85**	**48**	**-10.43**	36	-10.09	34	-10.29	24	-10.27	**53**	**-10.41**	21	-10.1	19	-10.37
ZINC36	7	-8.47	33	-9.91	44	-10.27	**48**	**-9.87**	35	-10.12	**31**	**-9.71**	29	-9.81	30	-10.07	22	-9.69
ZINC39	4	-8.97	32	-9.61	31	-9.28	38	-9.55	41	-9.37	25	-9.62	40	-9.58	**35**	**-9.44**	29	-9.49
ZINC41	9	-10.88	**42**	**-10.14**	43	-10.14	31	-10.3	28	-10.22	22	-9.95	41	-10.36	21	-9.64	28	-10.45

Note: Red bold font indicates the top most suitable ligand.

assigned to the protein atoms. It has been reported that Cys387, Val365, Tyr60, His132, Lys418, Gln334 and Asn385 residues are involved in catalysis and the interaction of their substrates (Bhutani et al. 2015), hence they are considered flexible residues for docking. The rest of the residues were treated as rigid and converted to autodock macromolecules. Grid preparations were performed using the AutoGrid tool of PyRx, where the grid box was designed in such a way that it could encompass all the flexible residues, with dimensions of 46 × 49 × 50. The grid spacing was set to 0.375 Å.

In this study, we performed 100 docking runs using the Lamarckian Genetic Algorithm (LGA) for each ligand. For Lamarckian GA, the parameters were set as 10 runs of each GA, the number of individuals in the population was set to 150, the maximum number of generations was set to 27,000, the rate of mutation was set to 0.02, the rate of crossover was set to 0.8, and other parameters were used as default values. Based on an Autodock scoring function, which was used to score the docked poses, the best conformation of each ligand was given the highest rank that also showed the least binding free energy. Adequate spaces of 0.25 Å for translation and 5 Å for rotation were chosen with a maximum energy evaluation of 2.5 × 106. All other docking parameters were set to their default values. Similarly, the above-mentioned docking protocol was used for all the mutant models considered in this study. Conformational clustering was performed on docked conformers with an RMSD tolerance of 1 Å. The top three most populated clusters were selected from each docking round of the mutant. The single lowest energy conformation was selected from the highest populated cluster and used for further interaction analysis.

Docking studies were done to focus on hydrogen bond interactions formed between the ligand and surrounding active site residues of DpRE1, along with van der Waals, hydrophobic and other interactions that may contribute to the stability of the protein–ligand complexes.

3. Results and Discussion

3.1. Structural modelling of DprE1 wild-type and its mutants

We have predicted the full-length structure of DprE1 with missing residues using homology modelling with the MODELLER 10.2 program, as described in Section 2.1. The stereochemical quality of the resultant structure was analysed using various tools on the SAVES and ProSA web server.

The Ramachandran plot of the model showed 94% residues in the favoured region and 4% residues in the allowed region, as shown in Figure 1c. ERRAT used to determine the quality of the model (Figure 1a) showed an overall quality factor of 91.49, which signifies an excellent quality of the predicted model (Colovos and Yeates 1993). The ProSA-Web Z-score of the model is -10.9 (Figure 1c), which indicates good model quality (Wiederstein and Sippl 2007). Also, the predicted knowledge-based energy used to evaluate the local model quality was found to be in the acceptable range. Overall, with a good quality score, the predicted homology model predominantly consists of sheets, helices, and coils with well-validated geometry. The superimposed structure of the predicted DprE1 model with the template model is shown in Figure 2, and the RMSD Cα value is 0.303 Å. This predicted homology model was used for the generation of mutants, which was followed by docking. Information related to the antibiotic resistant mutants of DprE1 was retrieved from the literature (Makarov et al. 2009; Neres et al. 2015; Foo et al. 2016). The seven mutant residues discussed in Section 2.1 (MutC387A, MutC387S, MutC387T, MutC387G, MutC387N, MutG17C and MutL368P) were individually incorporated in the predicted model at corresponding positions using Discovery Studio 3.5. Furthermore, a single model was prepared by incorporating all the mutant residues (Mut-All). All the mutant models, along with DprE1-WT and Mut-All were used for the docking studies.

3.2. Virtual screening of compounds against predicted DprE1 models

To characterise the binding mode of a known inhibitor, initially, the Y22 molecule co-crystalized with DprE1 (4P8C.pdb) was separated and redocked to check whether Autodock is able to reproduce the binding mode. The obtained RMSD value, 0.72 Å indicates the good reliability and consistency of the docking protocol (Maharaj et al. 2015; Barage et al. 2017; Meshram et al. 2020). Further, we analysed the molecular interactions of Y22 with DprE1, as depicted in Supplementary Material Figure S1. Also, the binding mode of the identified novel ligand molecules needs to be evaluated in comparison with the known ligands. Thus, to characterize the binding mode of the identified ligand molecules, molecular docking was used as described in Section 2.3. In total, 46 ligands were used for docking with the predicted DprE1-WT model and other mutant structures. The docked conformation for each ligand was subjected to conformational clustering with a RMSD tolerance of 1 Å.

3.3. Selection of top leads as DprE1 inhibitors

We docked each of the 46 ligand molecules with DprE1-WT, Mut-All, and the seven mutant models of DprE1. The number of highest populated clusters (HPC) and their

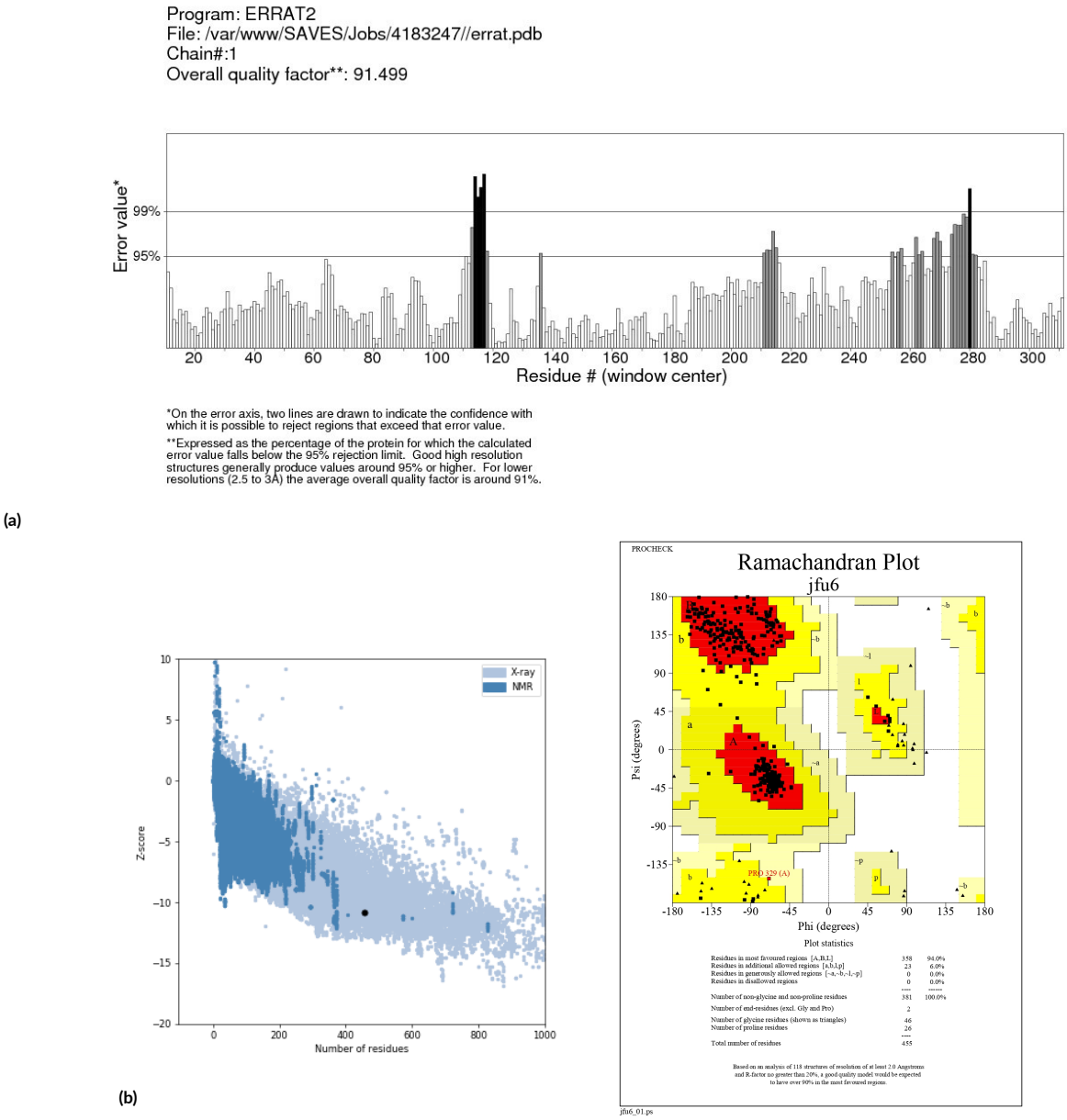

FIGURE 1 Protein model stereochemical quality assessment. a) ERRAT plot, b) ProSA-Web Z-score (black dot at -10.9), c) Ramachandran plot.

FIGURE 2 Superimposed structures of predicted DprE1 structure (purple) with template model (grey).

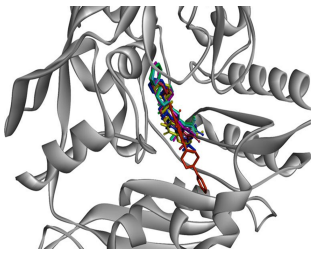

FIGURE 3 Superimposition of all docked ZINC5 conformations with Mut-All protein model.

corresponding binding energies (BE) were used for short-listing the leads. Conformational clustering of 46 ligand molecules docked with the DprE1-WT structure showed three highest populated clusters with 20, 16 and 15 conformations for the ligands ZINC5, ZINC8 and PBTZ169, respectively (See Supplementary Material Table S1 for ZINC IDs). The ligands ZINC5, ZINC8 and PBTZ169 corresponding to the highest populated clusters showed the lowest binding energies of –10.38, –10.25 and –9.08 kcal/mol, respectively. The molecular interactions of these ligand molecules with respect to the receptor were analysed. Similarly, the docked conformations of Mut-All and all other mutant structures were clustered based on an RMSD tolerance of 1 Å. From each docked complex, three lowest energy conformations were extracted from the highest populated clusters. Several ligand conformations were observed for their number of highest populated clusters and binding energies, as listed in Table 2. Furthermore, from all ligand molecules docked with all DprE1 structures, the top three docked conformations were analysed and evaluated for their binding mode in the catalytic groove of DprE1. Supplementary Material Table S1 enlists the ZINC IDs and their short forms as used in this study. We identified all the ZINC ligand molecules based on the similarity search with known inhibitors. So, the ZINC5 ligand has substructure similarity with the known inhibitor Benzothiazinone compound, which is used as an antitubercular drug (Karoli et al. 2012). Interestingly, among the top ligand molecules bound with

TABLE 2 Known inhibitor structures of DprE1 used for similarity search against ZINC database.

Inhibitor Name	Structures	Minimum Inhibitory Concentration (MIC) (in µM)	No. of similar ligands	Reference
PBTZ169	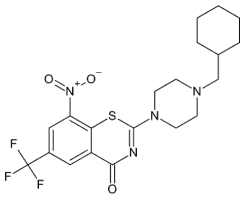	0.0006	1	(Panda et al. 2014)
BTZ043	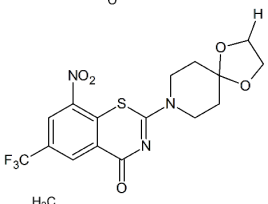	0.002	28	(Makarov et al. 2009)
Azaindole	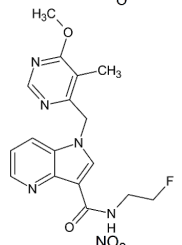	0.003	10	(Piton et al. 2017)
BTO	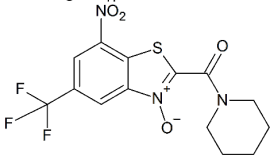	0.07	3	(Piton et al. 2017)

TABLE 3 Receptor-ligand interactions of the multiple drugs against the modelled DpRE1 targets.

S. No.	DprE1 models	Ligand	Amino acid residues interaction type							
			alkyl, pi-alkyl interactions	halogen interactions	pi-sigma interactions	H-bonding	pi-sulfur	pi-cation	pi-pi	pi-stacking
1	C387G	ZINC5	Ile131, Pro116, Ala417, Lys367, Arg58	Asn385, Ile386, Phe366, Val365	Val121	His132	-	-	-	-
2	C387G	ZINC28	Ile131, Pro116, Ala417, Lys367, Phe369, Val121, Tyr415	Gly125	-	His132, Tyr60, Lys 418, Cys129	Tyr415		-	-
3	C387G	ZINC17	Ile131, Pro116, Ala417, Lys367, Phe369, Ile131, Pro116, Ala417	-	-	-	-	Lys418	-	-
4	C387N	ZINC10	Ala417, Ile131, Val121, Cys129, Arg58	Gly133, His132	-	Lys418, His132, Gln336, Lys418, Tyr415	Tyr415	-	-	-
5	C387N	ZINC36	Ala417 , Lys367, Pro116	Arg58	-	Lys418, His132, Cys129	Ser228	-	Tyr415	-
6	C387N	BTZ043	Ala417, Pro116, Ile131, Tyr415, Lys367	Val365, Asn385, Phe366	-	Lys418, His132, Cys129	-	-	-	-
7	C387S	ZINC5	Val365, His132, Ala417, Ile131, Pro116,, Cys129, Val121, Arg58	Asn385, Val365	-	Lys418, His132, Ser387	Tyr415, Cys129	-	-	-
8	C387S	ZINC36	Val121, Arg58, Cys129, Ala417, Pro116	-	-	Lys418, His132, Ser59, Cys129	Tyr415	-	Tyr415	-
9	C387S	PBTZ169	-	-	-	Lys418, His132, Cys129	Tyr415	-	Tyr415	-
10	C387T	ZINC5	Lys367, Ile131, Pro116, Ala417, Arg58, Ala417	Phe366, Asn385, Val365, Phe366	Val121	Lys418, His132	Cys129	-	-	-
11	C387T	BTZ043	Lys367, Ala417, Ile131, Tyr415, Pro116	Phe366, Asn385	-	Lys418, His132	-	-	-	-
12	C387T	PBTZ169	Cys129, Arg58, Ala417, Lys367, Phe369	Arg58	-	Lys418, His132, Cys129	Tyr415	-	Tyr415	-
13	G17C	ZINC5	Phe369, Lys367, Ile131, Pro116, Ala417, Arg58	Asn385, Val365	Val121	His132, Lys418	Cys129	-	Tyr415	-
14	G17C	ZINC10	Phe369, Cys129, Ile131, Val121, Arg58, Ala417	His132	-	His132, Gly133	-	-	Tyr415	-
15	G17C	ZINC39	Pro116, Ile131, Ala417, Val121, Lys367	His132	-	Lys418	-	-	Tyr415	-
16	L368P	ZINC5	Ile131, Ala417, Arg58, Val121, Cys129, Val121, Arg58	Gln336	-	His132, Lys418, Tyr60	Cys129	-	Try415	-
17	L368P	ZINC28	Ile131, Ala417, Ile131, Val121, Lys367, Phe369	Gly125	-	His132, Ser59, Cys129	Try415	-	-	-
18	L368P	PBTZ169	Ile131, Ile131, Pro116, Val121, Arg58, Lys367	Gly125	Ala417	Lys418, Tyr60, His132, Ser59, Cys129	Try415	-	Try415	-
19	Wild-Type	ZINC5	Leu317, Leu363, Val365, Ile131, Cys129, Ala417	-	-	Lys418, Tyr415, Thr118, His132, Gln336	-	-	-	Tyr60
20	Wild-Type	ZINC8	Cys129, Ala417	Arg58	-	Lys418, Tyr415, Gln334, His132	-	-	Tyr415	-
21	Wild-Type	PBTZ169	Arg58, Ala417, Val121, Cys129, Ile131, Leu363, Val365, Cys387	-	-	Lys418, Tyr415, Tyr60, Gly117	-	-	-	-
22	C387A	ZINC5	Ala417, Cys129, Val121, Arg58	-	-	His132	Tyr415	-	Tyr415	-
23	C387A	ZINC28	Ala417, Val121, Lys367, Arg58	-	-	His132, Lys418, Ser59	Tyr415	-	Tyr415	-
24	C387A	ZINC41	Ala417, Ile131, Lys367	-	-	His132, Lys418, Cys129	Tyr415	-	Tyr415	-
25	Mut-All	ZINC5	Val121, Arg58, Ala417, Pro116, Cys129, Tyr415, His132	His132, Gln336, Asn385	Tyr415	His132, Lys418	Cys129, Tyr415	-	-	-
26	Mut-All	ZINC7	Val121, Tyr415, Ile131, Arg58, Cys129, Ala417, Phe369	-	Tyr415	His132, Gln336, Try415	Tyr415	-	-	-
27	Mut-All	ZINC17	Val121, Ala387, Lys367, Phe369, Ile131, Pro116	-	-	Thr118	-	Lys418	-	-

the nine DprE1 models, ZINC5 was found to be common in eight complexes, while PBTZ169 was common in four. Conversely, all other top three ligands were not observed in common with any docked complexes. Although the ligands ZINC5 and PBTZ169 were found to be common in multiple docked conformations, the top three ligands of all docked complexes were evaluated for their molecular interactions and the binding mode in the catalytic groove of DprE1 (Supplementary Material Figure S1). Our quest was to understand the substructure specificities of these ligands with the active site of DprE1 and to study the important residues involved in interactions with the ligand molecules.

The docked conformations of the ligands with the Gly17-Cys17 mutated model were subjected to conformational clustering analysis with a RMSD cut-off of 1 Å. The top 3 ligands, ZINC10, ZINC39 and ZINC5, showed the highest populated clusters with 35, 35 and 34 conformations, respectively. Similarly, the top 3 ligands for the Leu368-Pro368 mutated model were ZINC5, ZINC28 and PBTZ169, which showed the highest populated clusters with 58, 53 and 51 conformations, respectively. Since ZINC5 showed both better binding energy and a populated number of clusters, it was considered to be the best ligand. Similarly, for the Cys387-Ala387 mutated model, ZINC5, ZINC28 and ZINC42 were observed to have the highest populated clusters with 55, 44 and 42 conformations, respectively, where ZINC5 exhibited the best binding energy of –11.86 kcal/mol. Additionally, ZINC36, ZINC5 and PBTZ169 had the highest populated clusters of 31, 28 and 27 conformations, respectively, for the Cys387-Ser387 mutated model; for this model too, ZINC5 was selected owing to its better binding energy of –10.69 kcal/mol. For the Cys387-Thr387 model, BTZ043, PBTZ169 and ZINC5 showed the highest populated clusters with 64, 56 and 43 conformations, respectively. The binding energies of PBTZ169 (–10.36 kcal/mol) and ZINC5 (–10.12 kcal/mol) were found to be better as compared to the BTZ043 ligand. In the case of the Cys387-Gly387 model, ZINC5 showed the highest populated clusters and lowest binding energy of 54 and –11.12 kcal/mol, respectively, in comparison to ZINC28 and ZINC17. With respect to the Cys387-Asn387 mutated model, ZINC36, ZINC10 and BTZ043 exhibit the highest populated clusters of 48, 48 and 42 conformations, respectively. When all three residues, Gly17Cys, Leu368Pro, and Cys387Ala, were mutated (Mut-All), ZINC5 showed the lowest binding energy of –11.63 kcal/mol with the highest populated cluster of 35 conformations. Other top ligands were ZINC7 and ZINC17, with binding energies of –9.09 and –8.69 kcal/mol, respectively.

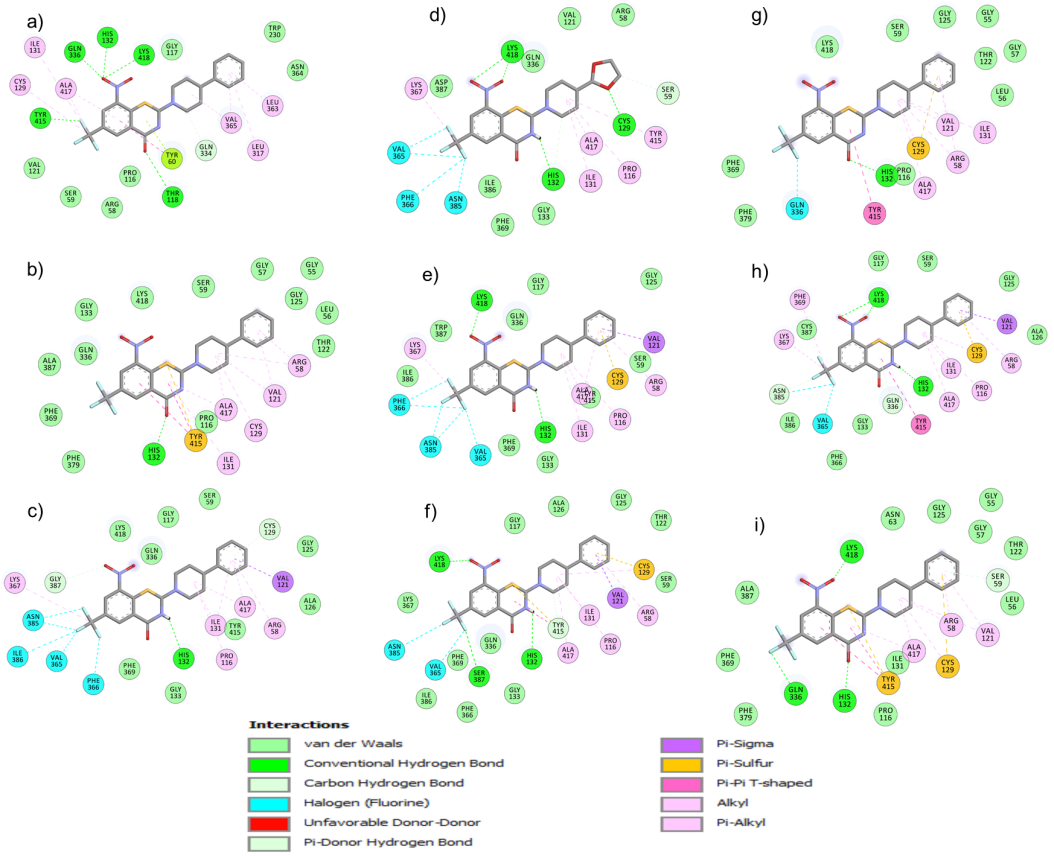

FIGURE 4 Two dimensional representation of the protein model with- top lead. a) Wild-type- ZINC5, b) C387A- ZINC5, c) C387G-ZINC5, d) C387N-BTZ043, e) C387T-ZINC5, f) C387S-ZINC5, g) L368P-ZINC5, h) G17C- ZINC5, i) Mut-All- ZINC5.

3.4. Interaction analysis of topmost leads

Molecular interactions of the top 3 ligand molecules were analysed to understand the substructure specificity and complementarity with the active site of Mut-All DprE1. All the bound conformations of ZINC5 were observed in the active site groove of the Mut-All DprE1 model, as depicted in Figure 3. In this section, we focus on the topmost lead identified in each protein model. The detailed interaction analysis of all protein models is provided in Supplementary Material.

Wild-Type: The top ligand molecule ZINC5 interaction with wild-type analysis revealed hydrogen bonding interactions with Thr118, His132 and Gln336 residues with the oxygen atoms. The residues Leu317, Leu363, Val365, Ile131, Cys129 and Ala417 show alkyl and pi-alkyl interactions with the ZINC5 molecule (Figure 4). Tyr60 forms pi-stacking interactions with the aromatic ring of ZINC5. Overall, an excellent interaction network of DprE1 residues has been observed with ZINC5 (Figure 5).

Cys387-Ala387: ZINC5 exhibits the best interactions with the C387A mutant model. Tyr415 shows a pi-sulfur interaction with the sulfur atom and also shows pi-pi T-shaped interactions with the aromatic rings of ZINC5 (Figure 4). Also, the His132 residue exhibits H-bonding interactions with the oxygen atom of ZINC5. Ala417, Cys129, Val121 and Arg58 form alkyl and pi-alkyl interactions with ZINC5 (Figure 5).

Cys387-Gly387: The interactions of ZINC5 with mutated model C387G have the best HPC and binding energy. The fluorine atom of ZINC5 makes halogen interactions with the residues Asn385, Ile386, Phe366 and Val365 (Figure 4). The residues Ile131, Pro116, Ala417, Lys367 and Arg58 also show alkyl and pi-alkyl interactions with the ZINC5 ligand molecule. Also, Val121 shows pi-sigma interactions with the aromatic ring of the ZINC5 ligand (Figure 5).

Cys387-Asn387: The topmost ligand interacting with the C387N mutant model is BTZ043. BTZ043 shows alkyl and pi-alkyl interactions with Pro116, Ile131, Ala417, Tyr415 and Lys367 residues (Figure 4 and Supplementary Material Figure S4). Val365, Asn385 and Phe366 show halogen interactions with the fluorine atoms of the BTZ043 ligand molecule. Cys129, Lys418 and His132 make hydrogen bonding interactions with the oxygen atom of BTZ043 (Figure 5).

Cys387-Thr387: ZINC5 is the top ligand that shows good interaction with the C387T mutant model. Val365, Asn385 and Phe366 form halogen bonds with fluorine atoms of ZINC5. The residues Lys367, Ile131, Pro116 and Ala417 show alkyl and pi-alkyl interactions with ZINC5 (Figure 4). Also, Val121 shows pi-sigma interaction, Arg58 and Ala417 show alkyl and pi-alkyl interaction, and Cys129 shows pi-sulfur interaction with the aromatic rings

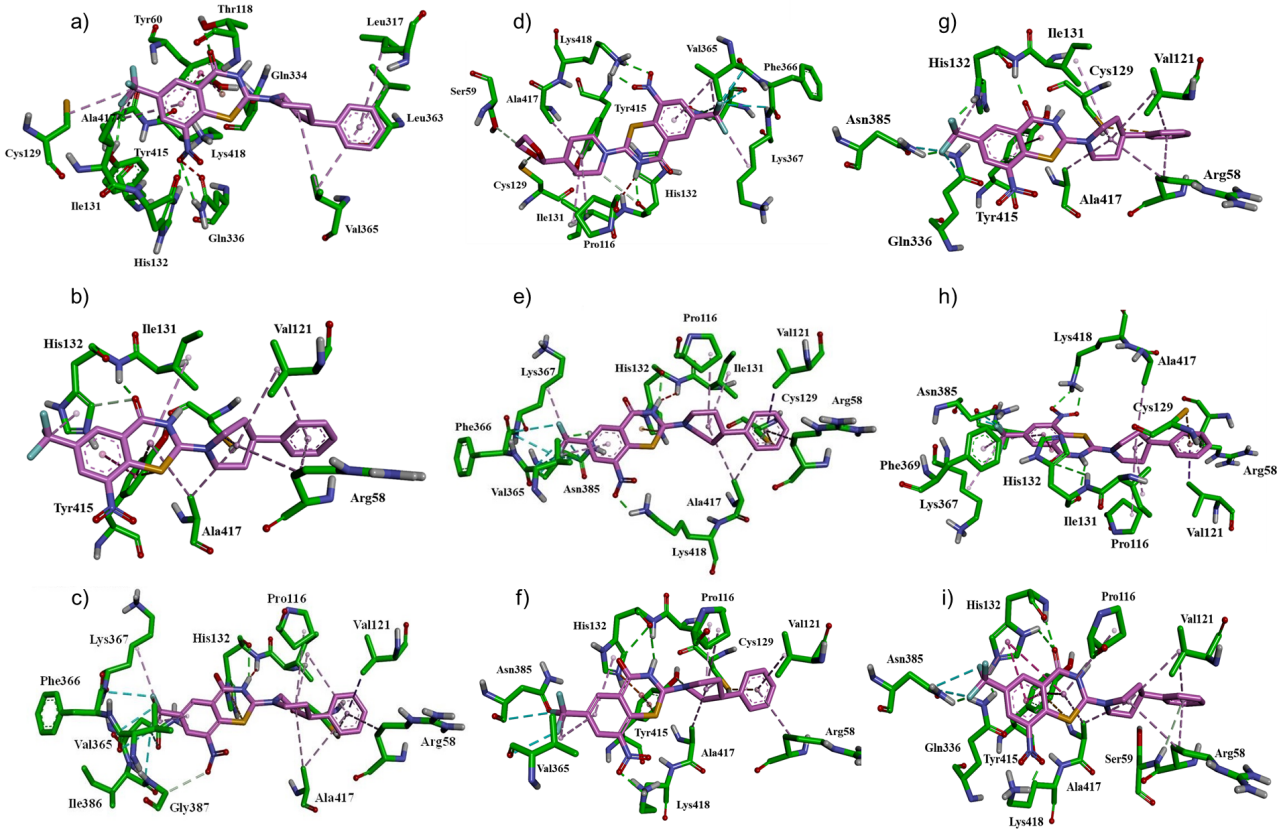

FIGURE 5 Three dimensional representation of the protein model with- top lead. a) Wild-type- ZINC5, b) C387A- ZINC5, c) C387G- ZINC5, d) C387N- BTZ043, e) C387T- ZINC5, f) C387S- ZINC5, g) L368P-ZINC5, h) G17C- ZINC5, i) Mut-All- ZINC5.

ZINC5 (Figure 5).

Cys387-Ser387: ZINC5 is the top ligand against the MutC387S model. Tyr415 shows a pi-sulfur interaction with the sulfur atom ZINC5. The fluorine atom exhibits H-bonding interactions with the Ser387 residue of ZINC5 (Figure 4). The fluorine atom of ZINC5 also makes halogen interactions with residues Asn385 and Val365. The residues Val365, His132, Ala417, Ile131, Pro116, and Cys129 interact by alkyl and pi-alkyl interactions with ZINC5. Also, Val121 and Arg58 show alkyl and pi-alkyl interactions, and Cys129 shows a pi-sulfur interaction with the aromatic ring of ZINC5 (Figure 5).

Leu368-Pro368: The fluorine atom of ZINC5 makes Halogen interactions with the Gln336 residue. The oxygen atom of ZINC5 makes H-bonding interactions with His132 residues (Figure 4). The residues Ile131, Ala417, Arg58, Val121 and Cys129 show alkyl and pi-alkyl interactions with the ZINC5 ligand molecule. Also, Val121 and Arg58 show alkyl and pi-alkyl interactions, and Cys129 shows pi-sulfur interactions with the aromatic rings of ZINC5. Try415 residue shows a pi-pi T-shaped interaction with ZINC5 (Figure 5).

Gly17-Cys17: The top ligand, ZINC5, shows a pi-pi T-shaped interaction with Tyr415 of the MutG17C model. His132 residue makes H-bonding interactions with the NH_2 group of ZINC5. The oxygen atom of ZINC5 makes H-bonding interactions with the Lys418 residue. The fluorine atom of ZINC5 makes Halogen interactions with residues Asn385 and Val365. The residues Phe369, Lys367, Ile131, Pro116 and Ala417 show alkyl and pi-alkyl interactions with ZINC5 (Figure 4). Also, Val121 shows pi-sigma interaction, Arg58 shows alkyl and pi-alkyl interaction, and Cys129 shows pi-sulfur interaction with the aromatic rings of ZINC5 (Figure 5).

Mut-All (Gly17Cys, Leu368Pro, Cys387Ala): The top ligand complexed with the Mut-All model is ZINC5. Val121, Arg58, Ala417 and Pro116 react with the carbon rings of ZINC5 via alkyl and pi-alkyl interactions. Cys129 shows pi-sulfur and pi-alkyl interactions with ZINC5 (Figure 4). Along with alkyl and pi-alkyl reactions and pi-sigma reactions with ZINC5, the Tyr415 residue also exhibits pi-sulfur interactions with the sulfur atom. His132 and Lys418 represent hydrogen bonding interactions with the oxygen atom of ZINC5. Also, His132 makes halogen interactions with the fluorine atom and forms alkyl and pi-alkyl interactions with the carbon atoms of ZINC5. Additionally, Gln336 and Asn385 residues exhibit halogen interactions with the fluorine atoms of the ZINC5 ligand (Figure 5).

Overall, molecular interactions were analysed for the top three ligands with the wild-type and all mutant structures of DprE1. We show that ZINC5 has better interaction chemistry than Y22 with wild and mutant DprE1 (Supplementary Material Figure S1 and Figure 4). Interestingly, the ZINC5 molecule was observed to efficiently accommodate in the active site of wild-type as well as all mutant structures of DprE1 (Figure 3). Furthermore, the interactions of DprE1 residues with the ZINC5 ligand in all the docked complexes were found to be conserved. In addition, the binding free energy of the ZINC5 ligand was found to be the lowest in most of the docked complexes. Whereas, compounds ZINC28 and ZINC17 has been found to be potential inhibitor for some mutant models.

4. Conclusions

In the present study, 3-dimensional structures of the DprE1 molecule were predicted using homology modelling and clinically relevant mutations were incorporated into the predicted structure at corresponding positions. The mutant models of DprE1 were subjected to energy minimization and were further used for docking studies. It was observed that the mutant structures did not exhibit a noticeable energy difference in comparison to the wild-type structure of DprE1, which indicates that the mutations did not affect the overall conformation and activity of the enzyme. The identified novel ligand molecules, along with known inhibitors, were screened against the wild-type and each mutant structure of DprE1. The results obtained from the docking studies revealed that the ZINC5 molecule possessed a good binding affinity towards the wild-type and all mutant structures of DprE1, except for MutC387N. The ZINC5 molecule was observed to have efficiently accommodated itself in the catalytic groove of DprE1. It depicted conserved hydrophobic and hydrophilic interactions with the key residues of DprE1 in all the docked conformations. Overall, the ZINC5 molecule can function as a potential inhibitor candidate against DprE1 inhibitor, which can overcome the resistance of *M. tuberculosis* towards contemporary antibiotic strategies. Further, experimental validation essential to test the efficacy of compound against DprE1 for its potential use as lead molecule.

Acknowledgments

Sagar Barage, Rajshri Singh and Anandakrishnan Karthic are grateful to Amity Institute of Biotechnology, Amity University, Mumbai, for providing necessary support for conducting the study.

Authors' contributions

SB and RS designed the study. CD, DM, AK carried out the laboratory work. CD, DM, AK, SB, RS analysed the data. DM, AK, SB, RS wrote the manuscript. All authors read and approved the final version of the manuscript

Competing interests

The authors declare no conflict of interest.

References

Barage S, Kulkarni A, Pal JK, Joshi M. 2017. Unravelling the structural interactions between PKR kinase domain and its small molecule inhibitors using computational approaches. J. Mol. Graph. Model. 75:322–329. doi:10.1016/j.jmgm.2017.06.009.

Barage S, Sonawane K. 2014. Exploring mode of phosphoramidon and Aβ peptide binding to hECE-1 by molecular dynamics and docking studies. Protein Pept. Lett. 21(2):140–152. doi:10.2174/09298665113209990091.

Bhat ZS, Rather MA, Maqbool M, Lah HU, Yousuf SK, Ahmad Z. 2017. Cell wall: A versatile fountain of drug targets in *Mycobacterium tuberculosis*. Biomed. Pharmacother. 95:1520–1534. doi:10.1016/j.biopha.2017.09.036.

Bhutani I, Loharch S, Gupta P, Madathil R, Parkesh R. 2015. Structure, dynamics, and interaction of *Mycobacterium tuberculosis* (Mtb) DprE1 and DprE2 examined by molecular modeling, simulation, and electrostatic studies. PLoS One 10(3):e0119771. doi:10.1371/journal.pone.0119771.

Colovos C, Yeates TO. 1993. Verification of protein structures: Patterns of nonbonded atomic interactions. Protein Sci. 2(9):1511–1519. doi:10.1002/pro.5560020916.

Dallakyan S, Olson AJ. 2015. Small-molecule library screening by docking with PyRx. Methods Mol. Biol. 1263:243–250. doi:10.1007/978-1-4939-2269-7_19.

Foo CSY, Lechartier B, Kolly GS, Boy-Röttger S, Neres J, Rybniker J, Lupien A, Sala C, Piton J, Cole ST. 2016. Characterization of DprE1-mediated benzothiazinone resistance in *Mycobacterium tuberculosis*. Antimicrob. Agents Chemother. 60(11):6451–6459. doi:10.1128/AAC.01523-16.

Hariguchi N, Chen X, Hayashi Y, Kawano Y, Fujiwara M, Matsuba M, Shimizu H, Ohba Y, Nakamura I, Kitamoto R, Shinohara T, Uematsu Y, Ishikawa S, Itotani M, Haraguchi Y, Takemura I, Matsumoto M. 2020. OPC-167832, a novel carbostyril derivative with potent antituberculosis activity as a DPRE1 inhibitor. Antimicrob. Agents Chemother. 64(6):e02020–19. doi:10.1128/AAC.02020-19.

Karoli T, Becker B, Zuegg J, Möllmann U, Ramu S, Huang JX, Cooper MA. 2012. Identification of antitubercular benzothiazinone compounds by ligand-based design. J. Med. Chem. 55(17):7940–7944. doi:10.1021/jm3008882.

Kim S, De Los Reyes V AA, Jung E. 2020. Country-specific intervention strategies for top three TB burden countries using mathematical model. PLoS One 15(4):e0230964. doi:10.1371/journal.pone.0230964.

Kyu HH, Maddison ER, Henry NJ, Ledesma JR, Wiens KE, Reiner R, Biehl MH, Shields C, Osgood-Zimmerman A, Ross JM, Carter A, Frank TD, Wang H, Srinivasan V, Abebe Z, Agarwal SK, Alahdab F, Alene KA, Ali BA, Alvis-Guzman N, Andrews JR, Antonio CAT, Atique S, Atre SR, Awasthi A, Ayele HT, Badali H, Badawi A, Barac A, Bedi N, Behzadifar M, Behzadifar M, Bekele BB, Belay SA, Bensenor IM, Butt ZA, Carvalho F, Cercy K, Christopher DJ, Daba AK, Dandona L, Dandona R, Daryani A, Demeke FM, Deribe K, Dharmaratne SD, Doku DT, Dubey M, Edessa D, El-Khatib Z, Enany S, Fernandes E, Fischer F, Garcia-Basteiro AL, Gebre AK, Gebregergs GB, Gebremichael TG, Gelano TF, Geremew D, Gona PN, Goodridge A, Gupta R, Bidgoli HH, Hailu GB, Hassen HY, Hedayati MT, Henok A, Hostiuc S, Hussen MA, Ilesanmi OS, Irvani SSN, Jacobsen KH, Johnson SC, Jonas JB, Kahsay A, Kant S, Kasaeian A, Kassa TD, Khader YS, Khafaie MA, Khalil I, Khan EA, Khang YH, Kim YJ, Kochhar S, Koyanagi A, Krohn KJ, Kumar GA, Lakew AM, Leshargie CT, Lodha R, MacArayan ERK, Majdzadeh R, Martins-Melo FR, Melese A, Memish ZA, Mendoza W, Mengistu DT, Mengistu G, Mestrovic T, Moazen B, Mohammad KA, Mohammed S, Mokdad AH, Moosazadeh M, Mousavi SM, Mustafa G, Nachega JB, Nguyen LH, Nguyen SH, Nguyen TH, Ningrum DNA, Nirayo YL, Nong VM, Ofori-Asenso R, Ogbo FA, Oh IH, Oladimeji O, Olagunju AT, Oren E, Pereira DM, Prakash S, Qorbani M, Rafay A, Rai RK, Ram U, Rubino S, Safiri S, Salomon JA, Samy AM, Sartorius B, Satpathy M, Seyedmousavi S, Sharif M, Silva JP, Silveira DGA, Singh JA, Sreeramareddy CT, Tran BX, Tsadik AG, Ukwaja KN, Ullah I, Uthman OA, Vlassov V, Vollset SE, Vu G, Weldegebreal F, Werdecker A, Yimer EM, Yonemoto N, Yotebieng M, Naghavi M, Vos T, Hay SI, Murray CJ. 2018. Global, regional, and national burden of tuberculosis, 1990-2016: Results from the global burden of diseases, injuries, and risk factors 2016 study. Lancet Infect. Dis. 18(12):1329–1349. doi:10.1016/S1473-3099(18)30625-X.

Laskowski RA, MacArthur MW, Moss DS, Thornton JM. 1993. PROCHECK: A program to check the stereochemical quality of protein structures. J. Appl. Crystallogr. 26(2):283–291. doi:10.1107/s0021889892009944.

Liu L, Kong C, Fumagalli M, Savková K, Xu Y, Huszár S, Sammartino JC, Fan D, Chiarelli LR, Mikušová K, Sun Z, Qiao C. 2020. Design, synthesis and evaluation of covalent inhibitors of DprE1 as antitubercular agents. Eur. J. Med. Chem. 208:112773. doi:10.1016/j.ejmech.2020.112773.

Maharaj Y, Bhakat S, Soliman M. 2015. Computer-aided identification of novel DprE1 inhibitors as potential anti-TB lead compounds: A hybrid virtual-screening and molecular dynamics approach. Lett. Drug Des. Discovery 12(4):302–313. doi:10.2174/1570180811666141001005536.

Makarov V, Manina G, Mikusova K, Möllmann U, Ryabova O, Saint-Joanis B, Dhar N, Pasca MR, Buroni S, Lucarelli AP, Milano A, De Rossi E, Belanova M, Bobovska A, Dianiskova P, Kordulakova J,

Sala C, Fullam E, Schneider P, McKinney JD, Brodin P, Christophe T, Waddell S, Butcher P, Albrethsen J, Rosenkrands I, Brosch R, Nandi V, Bharath S, Gaonkar S, Shandil RK, Balasubramanian V, Balganesh T, Tyagi S, Grosset J, Riccardi G, Cole ST. 2009. Benzothiazinones kill *Mycobacterium tuberculosis* by blocking arabinan synthesis. Science 324(5928):801–804. doi:10.1126/science.1171583.

Meshram RJ, Bagul KT, Pawnikar SP, Barage SH, Kolte BS, Gacche RN. 2020. Known compounds and new lessons: Structural and electronic basis of flavonoid-based bioactivities. J. Biomol. Struct. Dyn. 38(4):1168–1184. doi:10.1080/07391102.2019.1597770.

Neres J, Hartkoorn RC, Chiarelli LR, Gadupudi R, Pasca MR, Mori G, Venturelli A, Savina S, Makarov V, Kolly GS, Molteni E, Binda C, Dhar N, Ferrari S, Brodin P, Delorme V, Landry V, De Jesus Lopes Ribeiro AL, Farina D, Saxena P, Pojer F, Carta A, Luciani R, Porta A, Zanoni G, De Rossi E, Costi MP, Riccardi G, Cole ST. 2015. 2-carboxyquinoxalines kill *Mycobacterium tuberculosis* through noncovalent inhibition of DprE1. ACS Chem. Biol. 10(3):705–714. doi:10.1021/cb5007163.

Oh S, Trifonov L, Yadav VD, Barry CE, Boshoff HI. 2021. Tuberculosis drug discovery: A aecade of hit assessment for defined targets. Front. Cell. Infect. Microbiol. 11:611304. doi:10.3389/fcimb.2021.611304.

Panda M, Ramachandran S, Ramachandran V, Shirude PS, Humnabadkar V, Nagalapur K, Sharma S, Kaur P, Guptha S, Narayan A, Mahadevaswamy J, Ambady A, Hegde N, Rudrapatna SS, Hosagrahara VP, Sambandamurthy VK, Raichurkar A. 2014. Discovery of pyrazolopyridones as a novel class of noncovalent DprE1 inhibitor with potent antimycobacterial activity. J. Med. Chem. 57(11):4761–4771. doi:10.1021/jm5002937.

Piton J, Foo CS, Cole ST. 2017. Structural studies of *Mycobacterium tuberculosis* DprE1 interacting with its inhibitors. doi:10.1016/j.drudis.2016.09.014.

Sterling T, Irwin JJ. 2015. ZINC 15 - Ligand discovery for everyone. J. Chem. Inf. Model. 55(11):2324–2337. doi:10.1021/acs.jcim.5b00559.

The UniProt Consortium. 2021. UniProt: The universal protein knowledgebase in 2021. Nucleic Acids Res. 49(D1):D480–D489. doi:10.1093/nar/gkaa1100.

Webb B, Sali A. 2021. Protein Structure Modeling with MODELLER. Methods Mol. Biol. 2199:1–15. doi:10.1007/978-1-0716-0892-0_14.

Wiederstein M, Sippl MJ. 2007. ProSA-web: Interactive web service for the recognition of errors in three-dimensional structures of proteins. Nucleic Acids Res. 35(SUPPL.2):W407–10. doi:10.1093/nar/gkm290.

Wilsey C, Gurka J, Toth D, Franco J. 2013. A large scale virtual screen of DprE1. Comput. Biol. Chem. 47:121–125. doi:https://doi.org/10.1016/j.compbiolchem.2013.08.006.